frontiers | Frontiers in Bioengineering and Biotechnology

TYPE Original Research
PUBLISHED 15 January 2024
DOI 10.3389/fbioe.2023.1257669

OPEN ACCESS

EDITED BY
George Alexander Truskey,
Duke University, United States

REVIEWED BY
Aijun Qiao,
University of Alabama at Birmingham, United States
Milica Radisic,
University of Toronto, Canada
Michael T. Chin,
Tufts Medical Center, United States

*CORRESPONDENCE
Jianyi Zhang,
jayzhang@uab.edu

RECEIVED 12 July 2023
ACCEPTED 04 December 2023
PUBLISHED 15 January 2024

CITATION
Nguyen TM, Geng X, Wei Y, Ye L, Garry DJ and Zhang J (2024), Single-cell RNA sequencing analysis identifies one subpopulation of endothelial cells that proliferates and another that undergoes the endothelial-mesenchymal transition in regenerating pig hearts.
Front. Bioeng. Biotechnol. 11:1257669.
doi: 10.3389/fbioe.2023.1257669

Single-cell RNA sequencing analysis identifies one subpopulation of endothelial cells that proliferates and another that undergoes the endothelial-mesenchymal transition in regenerating pig hearts

Thanh Minh Nguyen[1], Xiaoxiao Geng[1], Yuhua Wei[1], Lei Ye[1], Daniel J. Garry[2] and Jianyi Zhang[1,3]*

[1]Department of Biomedical Engineering, University of Alabama at Birmingham, Birmingham, AL, United States, [2]Department of Medicine, School of Medicine, University of Minnesota, Minneapolis, MN, United States, [3]Department of Medicine, Cardiovascular Diseases, University of Alabama at Birmingham, Birmingham, AL, United States

Background: In our previous work, we demonstrated that when newborn pigs undergo apical resection (AR) on postnatal day 1 (P1), the animals' hearts were completely recover from a myocardial infarction (MI) that occurs on postnatal day 28 (P28); single-nucleus RNA sequencing (snRNAseq) data suggested that this recovery was achieved by regeneration of pig cardiomyocyte subpopulations in response to MI. However, coronary vasculature also has a key role in promoting cardiac repair.

Method: Thus, in this report, we used autoencoder algorithms to analyze snRNAseq data from endothelial cells (ECs) in the hearts of the same animals.

Main results: Our results identified five EC clusters, three composed of vascular ECs (VEC1-3) and two containing lymphatic ECs (LEC1-2). Cells from VEC1 expressed elevated levels of each of five cell-cyclespecific markers (Aurora Kinase B [AURKB], Marker of Proliferation Ki-67 [MKI67], Inner Centromere Protein [INCENP], Survivin [BIRC5], and Borealin [CDCA8]), as well as a number of transcription factors that promote EC proliferation, while (VEC3 was enriched for genes that regulate intercellular junctions, participate in transforming growth factor β (TGFβ), bone morphogenic protein (BMP) signaling, and promote the endothelial mesenchymal transition (EndMT). The remaining VEC2 did not appear to participate directly in the angiogenic response to MI, but trajectory analyses indicated that it may serve as a reservoir for the generation of VEC1 and VEC3 ECs in response to MI. Notably, only the VEC3 cluster was more populous in regenerating (i.e., $AR_{P1}MI_{P28}$) than non-regenerating (i.e., MI_{P28}) hearts during the 1-week period after MI induction, which suggests that further investigation of the VEC3 cluster could identify new targets for improving myocardial recovery after MI. Histological analysis of KI67 and EndMT marker PDGFRA demonstrated that while the expression of proliferation of endothelial cells was not significantly

different, expression of EndMT markers was significantly higher among endothelial cells of $AR_{P1}MI_{P28}$ hearts compared to MI_{P28} hearts, which were consistent with snRNAseq analysis of clusters VEC1 and VEC3. Furthermore, upregulated secrete genes by VEC3 may promote cardiomyocyte proliferation via the Pi3k-Akt and ERBB signaling pathways, which directly contribute to cardiac muscle regeneration.

Conclusion: In regenerative heart, endothelial cells may express EndMT markers, and this process could contribute to regeneration via a endothelial-cardiomyocyte crosstalk that supports cardiomyocyte proliferation.

KEYWORDS

single-nucleus RNA-sequencing, heart, angiogenesis, endothelial cells, cell cycle, autoencoder

1 Introduction

Adult mammal hearts, especially the cardiomyocytes, cannot regenerate (Laflamme and Murry, 2011; Steinhauser and Lee, 2011); after being damaged by an acute injury, such as myocardial infarction (MI), a large amount of cardiomyocytes die (Chiong et al., 2011). Although the adult and juvenile hearts may undergo remodeling (Sutton and Sharpe, 2000) to attempt repairing the damage, cardiomyocytes undergo pathological hypertrophy instead of proliferation, leading to further decrease of heart function, left ventricle dilation, and heart failure (McMullen and Jennings, 2007). No approach to reverse the post-MI pathological remodeling has been found; therefore, treatments of MI are only temporary, such as strengthening the heartbeat and increasing blood flow to the heart (Lu et al., 2015); and heart failure still frequently occurs (McMullen and Jennings, 2007). On the other hand, 4 weeks after MI was induced in postnatal (P) day 1, mammal hearts recovered completely by P30 with no decline in cardiac function and negligible myocardial scarring (Porrello et al., 2011; Ye et al., 2018; Zhu et al., 2018; Zhao et al., 2020); in these cases, cardiomyocytes robustly proliferated instead of becoming hypertrophic. Therefore, studying how neonatal hearts undergo 'regenerative' remodeling instead of 'failure' remodeling is important to find better treatment for MI and heart failure. Furthermore, We demonstrated that when apical resection (AR) surgery is performed in pig hearts on P1 (AR_{P1}), cardiomyocytes proliferated in response to MI induction on P28 (MI_{P28}), and the animals fully recovered with no evidence of scar formation and also no decline in heart function by P56 (Zhao et al., 2020; Nakada et al., 2022). Thus, we established a model where the juvenile hearts perform a 'regenerative' remodel to repair MI damage. Although inducing AR_{P1} may not be a therapeutic solution to prevent heart failure in mammals, this 'juvenile' regenerative model is more mature than the neonatal P1; therefore, understanding how different the cardiac cell types' regeneratively' respond to MI in this model may lead to better approaches for treating MI in adult hearts. The single nuclei RNA sequencing data (snRNAseq), which encompassed the gene expression of not only cardiomyocyte but also other cardiac cell types, were generated from these $AR_{P1}MI_{P28}$ regenerative hearts, the age-match naïve hearts (including embryonic day 80, postnatal P1, P28, and P56), and age-match non-regenerative hearts (MI_{P28} only) (Nakada et al., 2022). The cardiomyocyte snRNAseq data were analyzed in (Nguyen et al., 2022; Nguyen et al., 2023a) via our Autoencoder, and ten cardiomyocyte subpopulations were identified, one of which was present only in cardiomyocytes from AR_{P1} hearts on P28 and appeared to proliferate in response to MI (Nguyen et al., 2022); the subpopulation upregulated T-box transcription factors 5, 20 (TBX5 and TBX20), and erb-b2 receptor tyrosine kinase 4 (ERBB4), which were known to promote mouse cardiomyocyte proliferation (Bersell et al., 2009; Maitra et al., 2009; Chakraborty and Yutzey, 2012; Chakraborty et al., 2013; Misra et al., 2014; Xiang et al., 2016).

On the other hand, how the endothelial cells responded to MI in regenerative hearts was poorly studied. The primary function of the coronary vasculature is to deliver oxygen and nutrients to myocardial cells while removing waste products. The transport and transfer of these materials are facilitated by the endothelium. Thus, regeneration of the vessels that are damaged by MI is essential for minimizing the loss of pre-existing cardiac cells and promoting cardiac repair (Khurana et al., 2005; Ingason et al., 2018; Singh et al., 2022). The endothelial cells (ECs) that line the coronary vasculature are highly specialized for each vessel category (arteries, veins, capillaries, and lymph vessels) and for different segments within each category (Becker et al., 2023). Even adjacent ECs within the same vessel can display substantial phenotypic differences, and this heterogeneity is further exacerbated by myocardial injury. For the experiments described in this report, we used the Autoencoder to analyze snRNAseq data from ECs in the same animal hearts, and because ECs in the coronary vasculature rarely proliferate in healthy hearts but are robustly proliferative in response to injury (Potente et al., 2011), we focused our analyses on the angiogenic response to MI by restricting our cluster analysis to only the 1,646 genes included under the ontology term "cell cycle" in the Gene Ontology Resource (Gene Ontology Annotations, 2022). Our main hypothesis is whether EC subpopulations that highly expressed cell-cycle markers appeared in the regenerative heart data. Understanding through which molecules the EC increased proliferating, thus improving angiogenesis, may lead to new approaches in enhancing the vascular functions following MI. Also, we examined the potential mechanism of how EC subpopulations may crosstalk with signaling pathways in cardiomyocytes and promote cardiomyocyte proliferation, which is another contribution to deciphering heart regeneration.

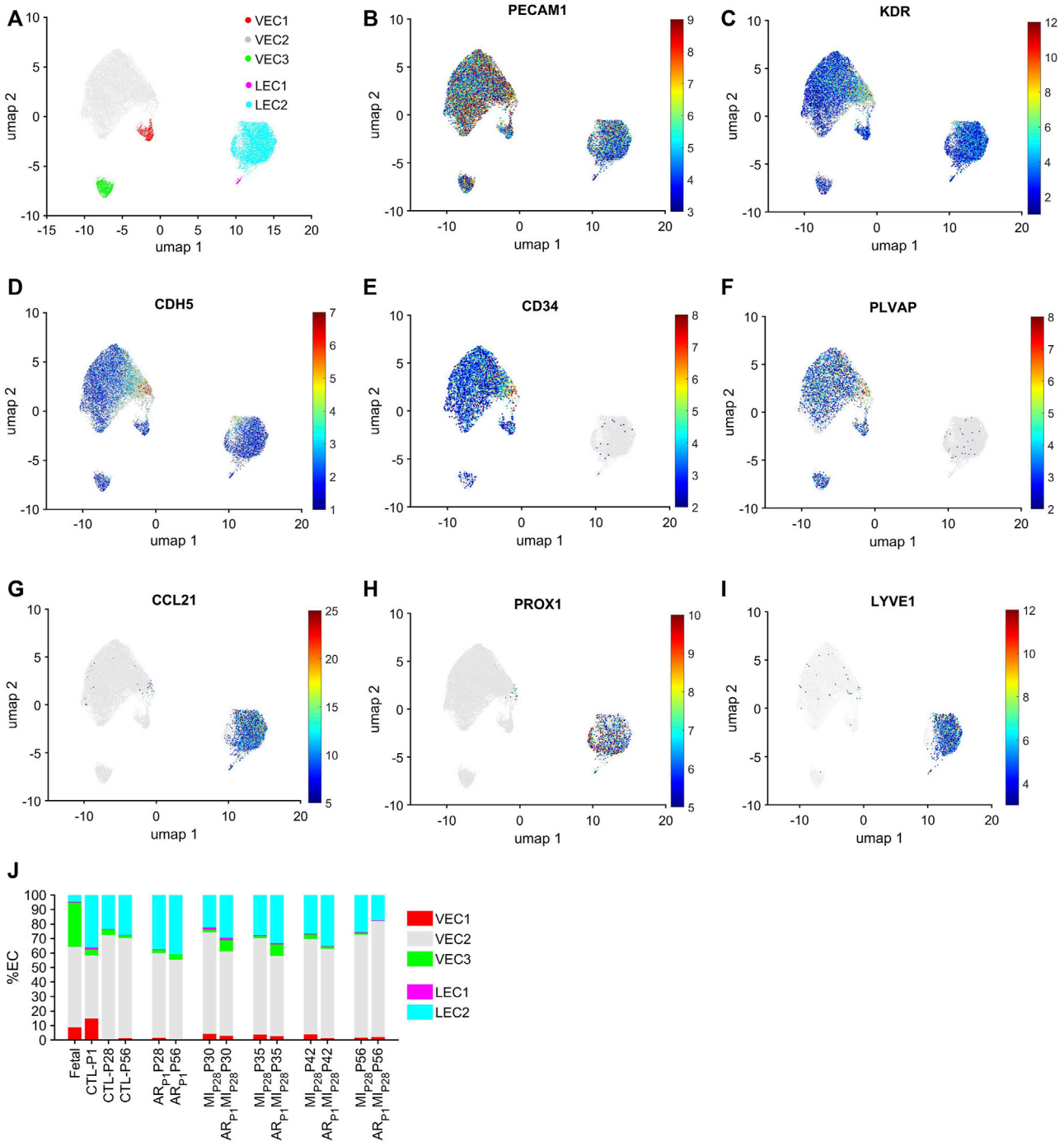

FIGURE 1
Cell-cycle specific Autoencoding defined five EC clusters in pig snRNAseq data. **(A)** Data for the expression of cell-cycle genes was extracted from the pig EC snRNAseq dataset, processed via an AI-based Autoencoder, and visualized in 2 dimensions (2D) via UMAP; the locations of each cluster are displayed. Cells that express the EC-specific markers **(B)** PECAM1, **(C)** KDR, and **(D)** CDH5; the VEC-specific markers **(E)** CD34 and **(F)** PLVAP; and the LEC-specific markers **(G)** CCL21, **(H)** PROX1 and **(I)** LYVE1 are displayed across the 2D cell-cycle–specific UMAP with the magnitude of expression represented as a color-coded heatmap; gray ECs did not express the corresponding molecule. **(J)** The proportion of ECs from each cluster is displayed for each injury group and time point.

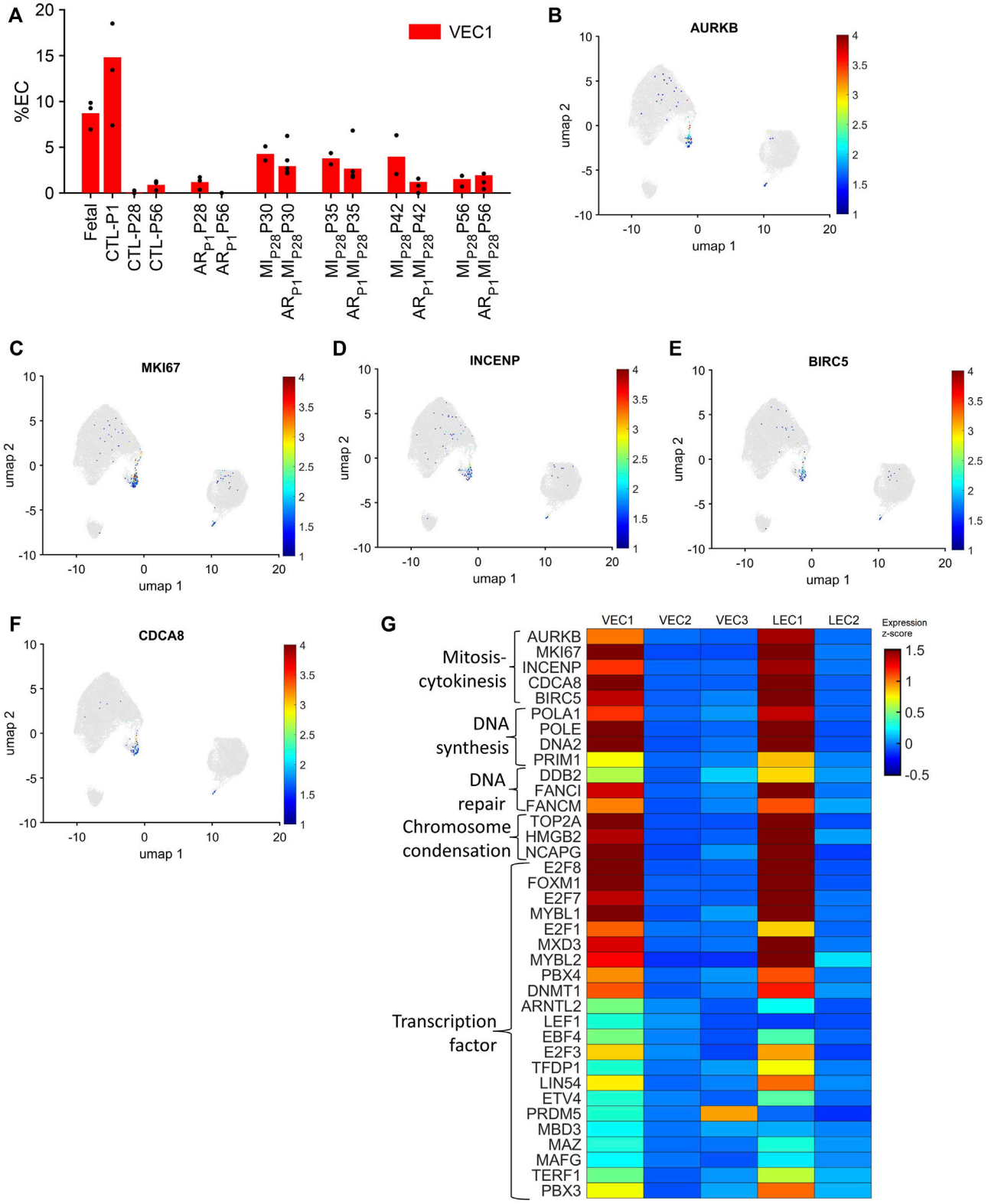

FIGURE 2
The VEC1 cluster is enriched for the expression of cell-cycle–related genes. **(A)** Data for VEC1 from Figure 1I is displayed with the *y*-axis rescaled for clarity. Cells that express the mitosis and cytokinesis markers **(B)** AURKB, **(C)** MKI67, **(D)** INCENP, **(E)** BIRC5, and **(F)** CDCA8 are displayed across the 2D cell-cycle–specific UMAP with the magnitude of expression represented as a color-coded heatmap; gray ECs did not express the corresponding molecule. **(G)** The abundance of expression for genes that are involved in mitosis and cytokinesis, DNA synthesis, DNA repair, and chromosome condensation, and for cell-cycle–regulating transcription factors is displayed for each cluster as a color-coded heat map (normalized by Seurat and converted to z-score).

TABLE 1 Summary of upregulated transcription factors in VEC1.

Transcription factor	Proportion of expressing cells (%)	Fold-change	*p*-value	References
E2F8	23.49	55.63	2.44×10^{-157}	Weijts et al. (2012)
FOXM1	22.11	42.54	4.58×10^{-132}	Zhao et al. (2006)
E2F7	15.89	27.14	1.57×10^{-89}	Weijts et al. (2012)
MYBL1	29.88	17.78	1.28×10^{-146}	Zhu et al. (2022)
E2F1	13.47	16.20	4.25×10^{-63}	Qin et al. (2006)
MXD3	21.07	14.89	4.56×10^{-89}	Diebold et al. (2019)
MYBL2	30.22	9.13	3.65×10^{-102}	
PBX4	19.34	8.35	1.60×10^{-55}	Martinou et al. (2022)
DNMT1	42.49	5.07	9.34×10^{-96}	Zhang et al. (2016)
ARNTL2	13.99	3.84	4.37×10^{-25}	
LEF1	10.19	3.09	1.59×10^{-12}	Planutiene et al. (2011)
EBF4	20.55	3.08	8.00×10^{-32}	
E2F3	51.47	3.08	6.77×10^{-82}	Zhou et al. (2013)
TFDP1	11.40	2.92	2.75×10^{-18}	
LIN54	49.91	2.87	3.05×10^{-72}	
ETV4	11.74	2.76	2.51×10^{-17}	Harel et al. (2021)
PRDM5	16.75	2.32	2.38×10^{-18}	
MBD3	10.19	2.26	2.34×10^{-13}	Yan et al. (2022)
MAZ	14.85	2.22	1.16×10^{-16}	Smits et al. (2012)
MAFG	11.74	2.07	3.31×10^{-13}	
TERF1	43.70	2.01	4.83×10^{-37}	
PBX3	80.66	2.01	2.43×10^{-62}	Chen et al. (2020), Wu et al. (2020)

Results are summarized as the proportion of VEC1 ECs that express the transcription factor, the fold-change in expression relative to expression in non-VEC1 ECs, and the *p*-value (Fisher's Exact test).

2 Results

2.1 Cell-cycle-specific AI autoencoding and cluster analysis of pig snRNAseq data identified five EC clusters

Pigs underwent AR_{P1}, MI_{P28}, $AR_{P1}MI_{P28}$, or neither surgical procedure (CTL). Subsequent experiments confirmed that pigs in the $AR_{P1}MI_{P28}$ group, but not MI_{P28} animals, completely regenerated the myocardial tissue that was damaged by MI (Zhao et al., 2020; Nakada et al., 2022). snRNAseq was performed with myocardial tissue collected from MI_{P28} and $AR_{P1}MI_{P28}$ animals on P30, P35, P42, and P56; from AR_{P1} and CTL animals on P28 and P56; from CTL animals on P1, and from fetal pigs.

The cell-cycle-specific Autoencoder (CSA) and clustering pipeline visualized five EC clusters (Figure 1A), each of which expressed elevated levels of the EC-specific surface markers Platelet And Endothelial Cell Adhesion Molecule 1 (PECAM1) (Newman, 1994), Kinase Insert Domain Receptor (KDR) (Terman et al., 1992), and vascular endothelial cadherin (CDH5) (Wu et al., 2021) (Figures 1B–D; Supplementary Figure S1). Three of the clusters were enriched for expression of the vascular-EC (VEC) markers CD34 (Fina et al., 1990) and Plasmalemma Vesicle Associated Protein (PLVAP) (Denzer et al., 2023) (Figures 1E, F), while the other two expressed high levels of the lymphatic-EC (LEC) markers C-C Motif Chemokine Ligand 21 (CCL21) (Johnson and Jackson, 2010), Prospero Homeobox 1 (PROX1) (Wigle et al., 2002), and Lymphatic Vessel Endothelial Hyaluronan Receptor 1 (LYVE1) (Banerji et al., 1999) (Figures 1G–I). Thus, the CSA appeared to separate the global cardiac EC population into three clusters of vascular ECs (VEC1-3) and two clusters of lymphatic ECs (LEC1-2).

Each EC cluster contained cells from multiple experimental groups and time points (Supplementary Figure S2), confirming that our results were not compromised by sampling bias. Further, we verified that the results were not compromised by batch effects. VEC1-3 collectively comprised >95% of ECs in fetal hearts and 59%–81% of ECs in hearts from all nonfetal animal groups (Figure 1J), whereas LEC1-2 included the remaining <5% of ECs in fetal hearts and 19%–41% of ECs in nonfetal hearts. The majority of VECs were clustered in VEC2, regardless of animal groups or time points, with the highest proportions of VEC1 and VEC3 ECs observed in CTL hearts on P1 and in fetal hearts, respectively. Nearly all LECs were clustered in LEC2.

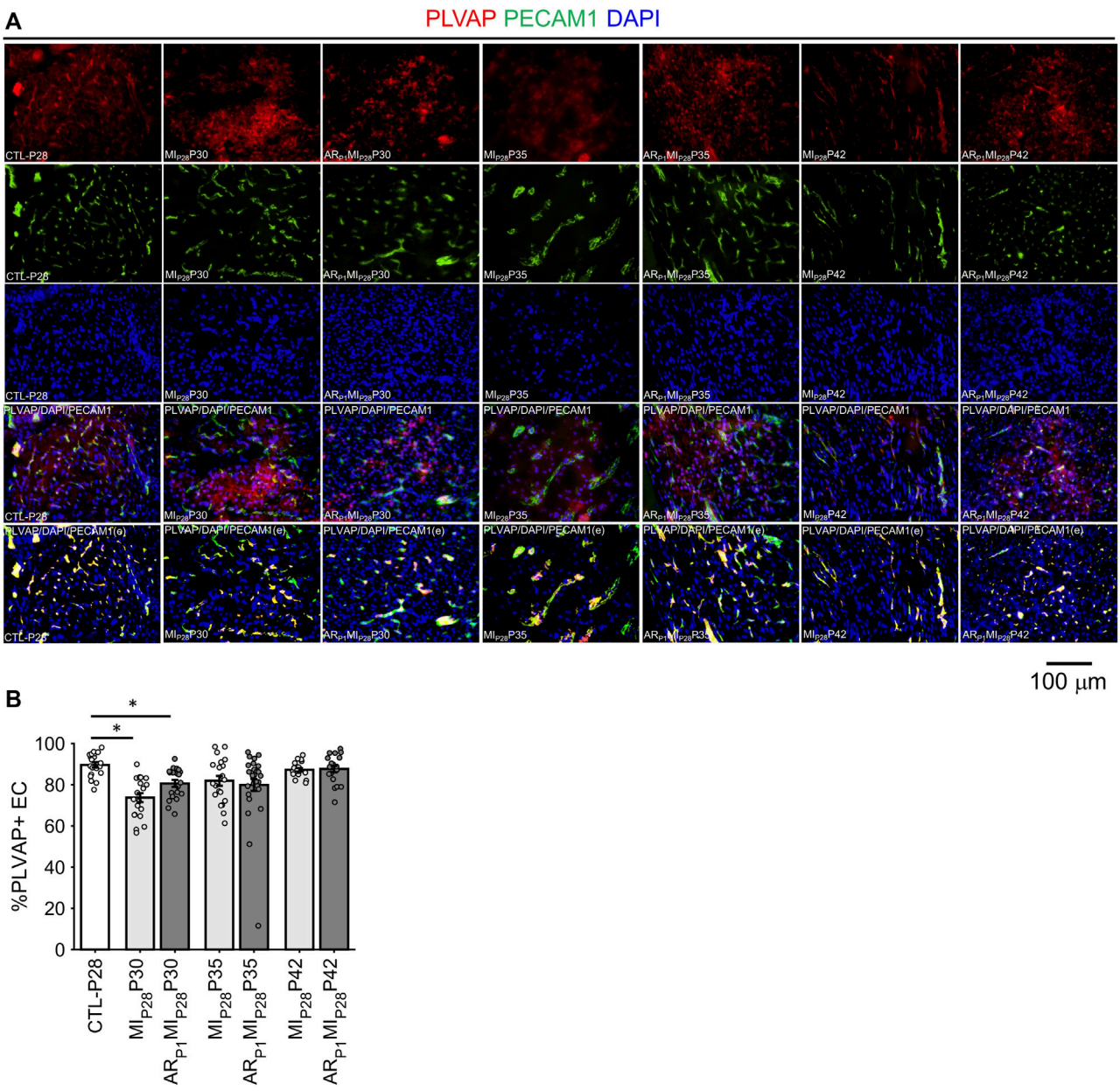

FIGURE 3
Fluorescence immunostaining analysis to assess ing the percentage of PLVAP + endothelial cells (VEC marker) in all animal group. **(A)** Representative images; the number of endothelial cells, marked by the DAPI blue fluorescence overlapping with EC marker PECAM1 green fluorescence, was counted; then, PLVAP red fluorescence and green fluorescence was amplified by 2x; red the signal not overlapping with green was removed before merging with DAPI (PLVAP/DAPI/PECAM(e) channel) to enhance PLVAP + EC visualization and counting. **(B)** Percentage of PLVAP + EC in all animal groups; the horizontal bar and the star (*) indicates non-parametric Wilcoxon's ranksum test between two sample groups. *: p-value < 0.05.

2.2 VEC1 was enriched for the expression of genes involved in cell-cycle activity and proliferation

VEC1 ECs comprised 8.7% of ECs in fetal hearts and 14.8% of ECs in CTL hearts on P1, they declined to nearly undetectable levels in CTL hearts on P28, and then expanded to include 3.5%–4.2% of ECs in MI_{P28} hearts from P30-P42 and in $AR_{P1}MI_{P28}$ hearts on P30-P35 (Figure 2A). VEC1 was also the only VEC cluster to express elevated levels of each of five markers for mitosis and cytokinesis (Aurora Kinase B [AURKB], marker of proliferation Ki-67 [MKI67], Inner Centromere Protein [INCENP], Survivin [BIRC5], and Borealin [CDCA8] (Li et al., 1998; Vader et al., 2006); Figures 2B–G; Supplementary Figure S3) and was enriched for the expression of genes associated with DNA synthesis and repair (Gene Ontology Annotations, 2023b), chromosome condensation (Gene Ontology Annotations, 2023c), and the gene ontology terms DNA replication ($p = 3.86 \times 10^{-8}$), mitotic spindle organization ($p = 8.71 \times 10^{-7}$), and mitotic cytokinesis ($p = 2.42 \times 10^{-6}$) (Figure 2G; Supplementary Tables S1A, B), as well as numerous transcription

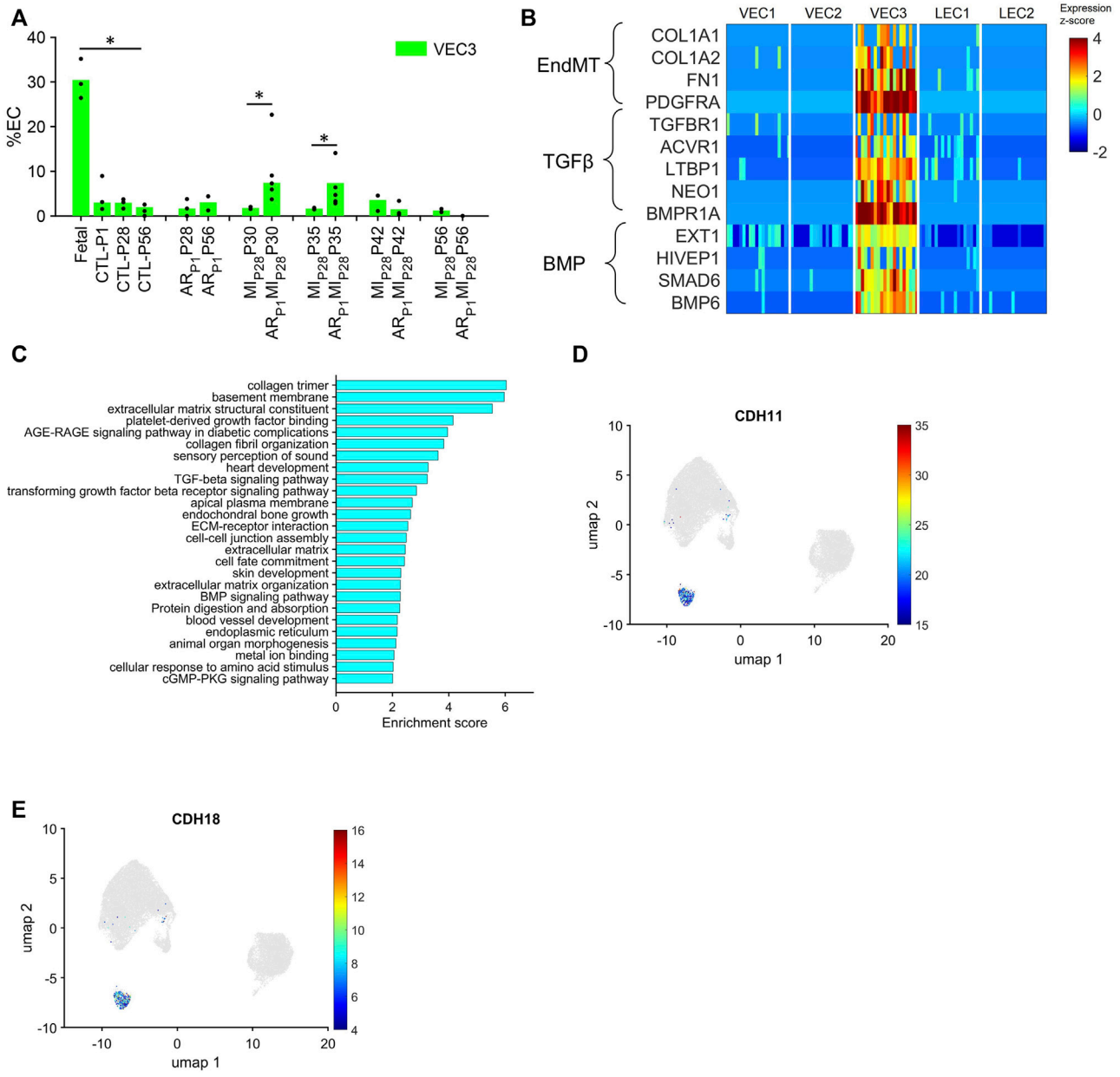

FIGURE 4
The VEC3 cluster is enriched for the expression of genes involved in the EndMT and cell adhesion. **(A)** Data for VEC3 from Figure 1I is displayed with the *y*-axis rescaled for clarity (*$p < 0.05$, Wilcoxon-ranksum test). **(B)** The abundance of expression for genes that are involved in the EndMT, in Transforming Growth Factor β signaling, and in Bone Morphogenetic Protein signaling (BMP) is displayed for each cluster as a color-coded heat map (normalized by Seurat and converted to z-score). **(C)** Enrichment scores (base-10 logarithm of enrichment *p*-value) were calculated for ECs from the VEC3 cluster and evaluated with the DAVID functional analysis tool; the 26 most highly enriched ontologies/pathways ($p < 0.01$) are displayed. **(D,E)** Cells that express the adhesion molecules **(D)** CDH11 and **(E)** CDH18 are displayed across the 2D cell-cycle–specific UMAP with the magnitude of expression represented as a color-coded heatmap; gray ECs did not express the corresponding molecule.

factors that have been linked to increases in EC proliferation and angiogenesis (Figure 2G; Table 1). Collectively, these observations are consistent with previous reports that the coronary vasculature undergoes a period of rapid growth and remodeling shortly after birth (Tian et al., 2014; Tan and Lewandowski, 2020) and suggest that a small proportion of cardiac ECs revert to a more proliferative phenotype in response to MI on P28.

Notably, although LEC1 ECs were exceptionally rare (<1.5%) in hearts from all groups and time points, they were most abundant in CTL hearts on P1 and in MI_{P28} and $AR_{P1}MI_{P28}$ hearts on P30 (Figure 1I; Supplementary Figure S4), and were enriched for many of the same mitosis/cytokinesis markers, gene ontology terms, and transcription factors that were upregulated in VEC1 ECs (Figure 2G), which suggests that expansion of the LEC1 cluster may have a role in the inflammatory response (Prabhu and Frangogiannis, 2016) and/or contribute to the re-uptake of interstitial fluid after MI. Also, Immunohistological staining of VEC clusters' markers (PLVAP + PECAM1) (Figure 3) showed

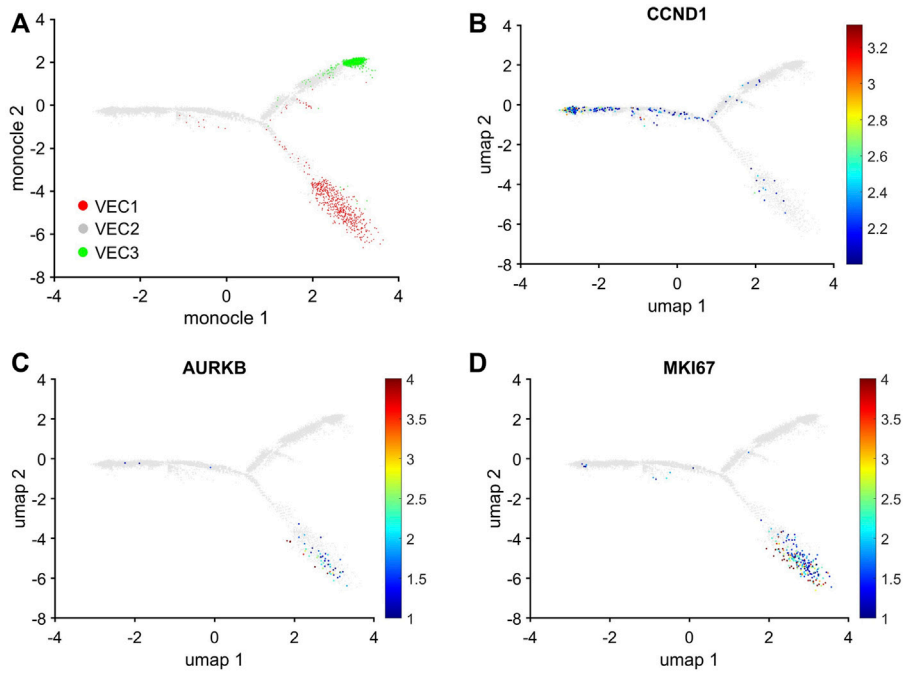

FIGURE 5
Trajectory analysis of pig EC snRNAseq data identified pathways between VEC2 and VEC1 or VEC3, but not between VEC1 and VEC3. Trajectory analysis of cell-cycle gene expression in VEC1, VEC2, and VEC3 ECs was performed via Monocle. **(A)** The positions of cells from each of the three VEC clusters is displayed across the trajectory. ECs that express **(B)** CCND1, which regulates the G1/S phase transition, and the proliferation markers **(C)** AURKB and **(D)** MKI67 are displayed across the 2D cell-cycle–specific UMAP with the magnitude of expression represented as a color-coded heatmap; gray ECs did not express the corresponding molecule.

that on P30, the percentage of PLVAP + ECs significantly decreased, compared to CTL-P28 level as the baseline, following MI_{P28} in both regenerative ($p = 3.382 \times 10^{-4}$) and non-regenerative heart ($p = 3.4995 \times 10^{-6}$); then, these percentage returned to the baseline level on P42. Since the percentages of VEC and LEC clusters were complemented, this result also suggested an increase of LEC between 2 and 7 days after MI_{P28}. This LEC expansion was also suggested by an increase of cycling LEC1 cluster found in the snRNAseq analysis. Besides, trajectory analysis of LEC clusters (Supplementary Figure S4) also showed continuous paths from LEC2 to LEC1; the ordered was from cell-cycle G1/S phase marker Cylin D1 (CCND1) through S-phase marker CCNE2, M-phase marker CCNB2, to proliferation marker MKI67.

2.3 VEC3 was enriched for the expression of genes involved in cell adhesion, the regulation of intercellular junctions, and the endothelial-mesenchymal transition (EndMT)

Although VEC1 ECs became more common in pig hearts after MI was induced on P28, they tended to be *less* common (though not significantly) in $AR_{P1}MI_{P28}$ hearts than in MI_{P28} hearts from P30-P42 and, consequently, are unlikely to contribute to the enhanced regenerative potential observed in the hearts of $AR_{P1}MI_{P28}$ pigs. Conversely, the VEC3 cluster was significantly *more* prominent in fetal (30.46%) than CTL hearts (3.9%–2.0% from P1-P56; $p < 0.05$ at each time point) and in $AR_{P1}MI_{P28}$ hearts than in MI_{P28} hearts on P30 ($AR_{P1}MI_{P28}$: 6.33%, MI_{P28}: 1.6%; $p < 0.05$) and P35 ($AR_{P1}MI_{P28}$: 6.86%, MI_{P28}: 1.8%; $p < 0.05$) (Figure 4A), but was *not* enriched for the expression of mitosis/cytokinesis markers (Figure 2G; Supplementary Table S2A). Instead, VEC3 ECs expressed elevated levels of genes associated with the EndMT, with the Transforming Growth Factor β (TGFβ) and Bone Morphogenetic Protein (BMP) (Figure 4B; Supplementary Table S2B) pathways (Huang et al., 2022; Gene Ontology Annotations, 2023a; KEGG, 2023), and with ontology terms that are associated with the upregulation of blood-vessel development (Figure 4C; Supplementary Table S2B). Notably, both TGFβ and BMP signaling regulate the EndMT, and although the EndMT appears to contribute to the formation of a number of pathological vascular abnormalities (Huang et al., 2022), all three processes are crucial for embryonic cardiovascular development (Gordon and Blobe, 2008; Morrell et al., 2016; Kovacic et al., 2019). Furthermore, VEC3 ECs expressed elevated levels of Plakophilin 2 (PKP2, fold-change: 24.62, p-value: 5.74×10^{-247}), which regulates the assembly of intercellular junctions (Bass-Zubek et al., 2008), as well as the adhesion molecules Cadherin 11 (CDH11) and Cadherin 18 (CDH18) (Figures 4D, E; Supplementary Figure S5), while expression of the junctional proteins KDR and CDH5 (Giannotta et al., 2013) was somewhat lower in VEC3 than in VEC1 ECs (Supplementary Figure S1).

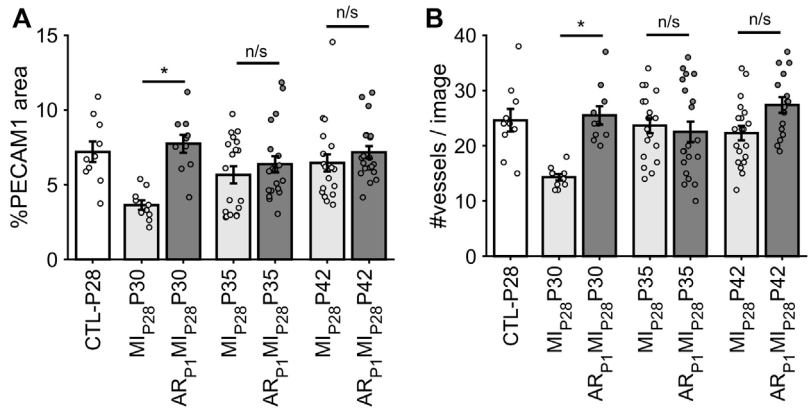

FIGURE 6
Estimating vessel density in each animal group via fluorescence immunostaining. **(A)** For each image, the percentage of pixel having PECAM1 green fluorescence was counted. **(B)** For each image, the number of vessels was manually counted. The horizontal bar and the star (*) indicates non-parametric Wilcoxon's ranksum test between two sample groups. *: p-value <0.05; ns: p-value ≥ 0.05.

2.4 Trajectory analysis linked VEC2 to VEC1 and VEC3, but there was no direct pathway between VEC1 and VEC3

The uniqueness of the VEC1 and VEC3 clusters was also evidenced by the results from Monocle pseudotime trajectory analysis (Qiu et al., 2017) of cell-cycle snRNAseq data for cells in all three VEC clusters. The analysis produced a branched structure with the tips of two branches each composed almost exclusively of VEC1 or VEC3 ECs and the third branch, as well as the region where all three branches converged, occupied by primarily VEC2 ECs (Figure 5A). Furthermore, the distribution of cells expressing Cyclin D1 (CCND1), which regulates the G1/S phase transition, and the proliferation markers AURKB and MKI67 traced a pathway between VEC2 and VEC1, but not between VEC2 and VEC3 or VEC3 and VEC1 (Figures 5B–D). Collectively, these observations indicated that VEC2 ECs could transform into either VEC1 or VEC3 ECs, but there was no direct transformational pathway between the VEC1 and VEC3 clusters, and identified a trajectory from VEC2 to VEC1 that recapitulated the onset and progression of cell-cycle activity and proliferation.

2.5 Angiogenesis (vessel density and proliferation marker)

Following MI$_{P28}$, the vessel density, quantified by the percentage of image PECAM1 area and by the manual counting of vessels in each image (Figure 6), significantly decreased on P30 in non-regenerative hearts; then, on P35 and P42, their vessel densities recovered to the level of CTL-P28 hearts. Meanwhile, in regenerative hearts, the vessel densities did not significantly change, remaining similar to CTL-P28. On the other hand, Marker of Proliferation Ki67 immunofluorescence analysis (Figure 7) showed that seven to 14 days following the MI$_{P28}$ injury, endothelial cells in both regenerative and non-regenerative hearts actively proliferate. Before the injury, less than 1% of EC expressed Ki67. Then, on day 7 and 14 after MI$_{P28}$, the percentages of Ki67+ EC increased to, and remained between 6% and 8% in the non-regenerative hearts (MI$_{P28}$P35 and MI$_{P28}$P42, respectively); meanwhile, in the regenerative hearts, % Ki67+ EC increased to 9.88% on P35, then decreased to 5.20% on P42. The difference of Ki67+ EC between the two groups was insignificant at these time points (p = 0.062 and p = 0.467, respectively), and was consistent with the snRNAseq analysis. Then, we compared the expression of Vascular Endothelial Growth Factor A (VEGFA) and Vascular Endothelial Growth Factor B (VEGFB), which are known as the driver genes in angiogenesis involved in wound healing (Johnson and Wilgus, 2014), in the whole-heart snRNAseq data. Supplementary Figure S6 showed that it was unclear whether these two genes expressions were consistently higher in the regenerative (or on-regenerative) groups. This observation may explain why we did not observe significant angiogenesis between the regenerative and non-regenerative hearts.

2.6 VEC3 markers PDGFRA are highly expressed in ECs of regenerative hearts up to 7 days following MI$_{P28}$ injury

In Figure 8, the expression of EndMT marker PDGFRA in EC was represented by the intensity of red fluorescence overlapping with green (EC marker PECAM1) fluorescence. A small number (~1.5%) of EC in the CTL-P28 hearts were VEC3; therefore, the PDGFRA expression in CTL-P28 EC was used as the baseline. Then, following MI$_{P28}$ injury, PDGFRA expression in the non-regenerative hearts EC sharply decreased on P30, then gradually increased on P35 and P42; however, the

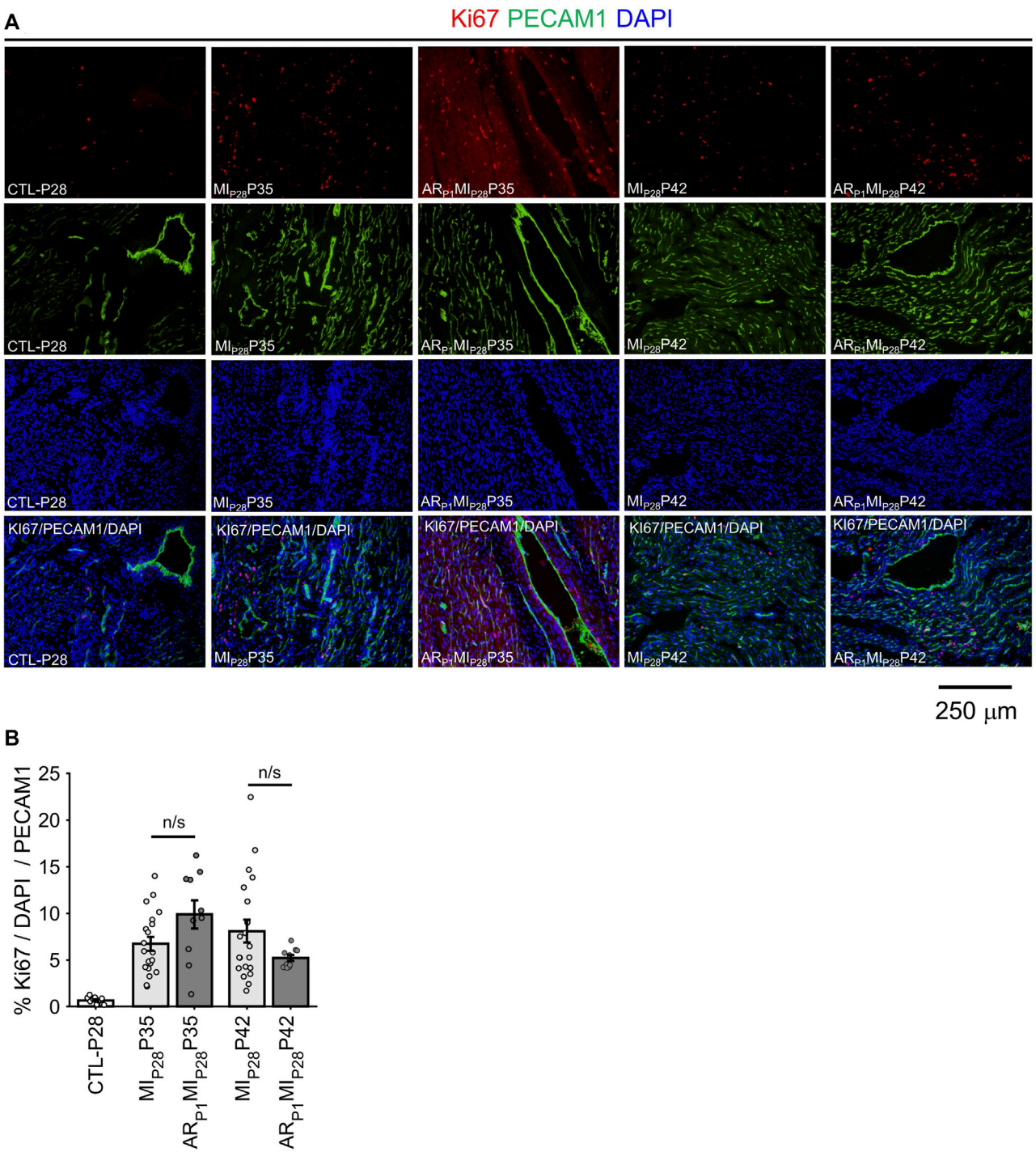

FIGURE 7
Immunofluorescence analysis confirming EC proliferation. **(A)** Representative images of Ki67 (red)/PECAM1 (green)/DAPI (blue) in each group. **(B)** For each image, the percentage of KI67+ EC was manually counted. The horizontal bar and the star (*) indicates non-parametric Wilcoxon's ranksum test between two sample groups. ns: p-value ≥ 0.05.

increased expression did not reach beyond the baseline level. Meanwhile, PDGFRA expression sharply increased in the regenerative heart on P30 ($p = 7.69 \times 10^{-4}$) and P35 ($p = 4.71 \times 10^{-5}$), then reverted to the baseline level on P42. These trends were consistent with the snRNAseq analysis. Also, surprisingly, PDGFRA immunofluorescence analysis showed that non-endothelial cells surrounding PDGFRA + EC also expressed PDGFRA; these cells could be cardiac fibroblasts and cardiomyocytes, as reported in (Bloomekatz et al., 2017; Yao et al., 2022).

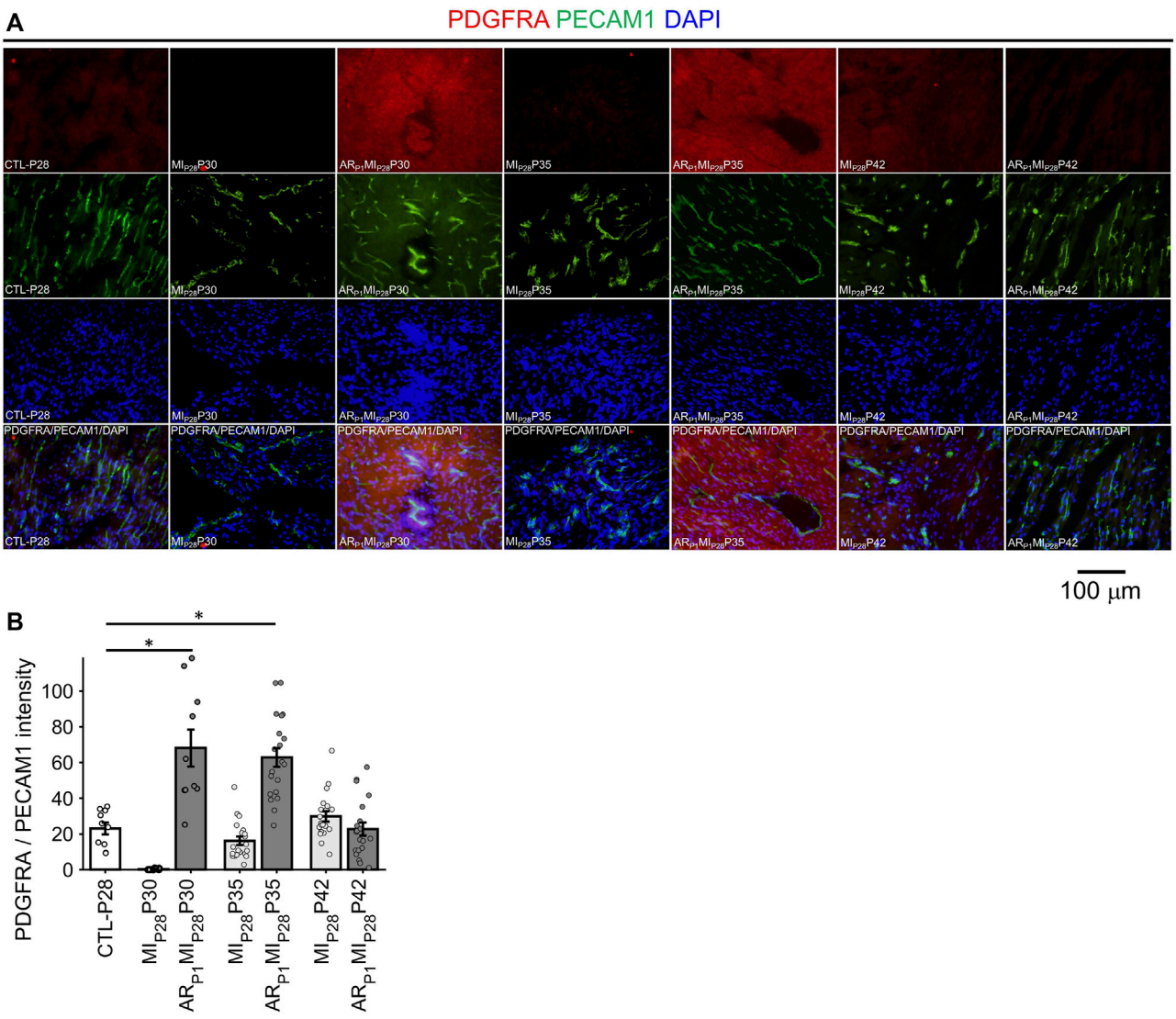

FIGURE 8
Fluorescence immunostaining analysis to confirm PDGFRA (EndMT marker) expression in endothelial cells. **(A)** Representative images of PDGFRA (red)/PECAM1 (green)/DAPI (blue) in each group. **(B)** The expression of PDGFRA was represented by the average PDGFRA red light intensity that are overlapped with EC marker green regions. The horizontal bar and the star (*) indicates non-parametric Wilcoxon's ranksum test between two sample groups. *: p-value < 0.05.

2.7 VEC3 upregulated genes encoding secretable proteins that may promote cardiomyocyte proliferation and heart regeneration via Pi3k-Akt, Hippo/YAP, and ERBB4 signaling pathways

Our previous works demonstrated the upregulation of Hippo/YAP signaling pathway in regenerative pig hearts that underwent myocardial infarction on P1 (Zhang et al., 2020), as well as ERBB4 in AR_{P1}P28 hearts (Nguyen et al., 2022) at the protein level. Also, Pi3k-Akt signaling pathway was found enriched in $AR_{P1}MI_{P28}$ cardiomyocytes (Nakada et al., 2022; Nguyen et al., 2023b). Therefore, we examined whether the VEC3 cluster may have genes that interact with these pathways (Figure 9A). Thirty genes encoding secretable proteins were found upregulated in VEC3; among them, Fibronectin 1 [FN1] (Wang et al., 2013), Neuregulin 1 [NRG1] (Bersell et al., 2009; Gemberling et al., 2015), Versican [VCAM] (Feng et al., 2023), and Periostin [POSTN] (Kuhn et al., 2007) were known to promote cardiomyocyte proliferation in zebrafish, mice, and rat. We also queried the protein-protein interactions between these 30 genes and their receptors linked to Pi3k-Akt, Hippo/YAP, and ERBB4 signaling pathways in the Biological General Repository for Interaction Datasets (BioGrid) (Oughtred et al., 2021). Figure 9B shows that POSTN, FN1, and VCAM interact with Integrin Alpha 1 [ITGA1] and Integrin Beta 1 [ITGB1], which are receptors of the Pi3k-Akt signaling pathway (Feng et al., 2023). Also, Fibrillin 2 [FBN2], which was upregulated in VEC3, interact with Insulin Receptor [INSR] of Pi3k-Akt signaling pathway.

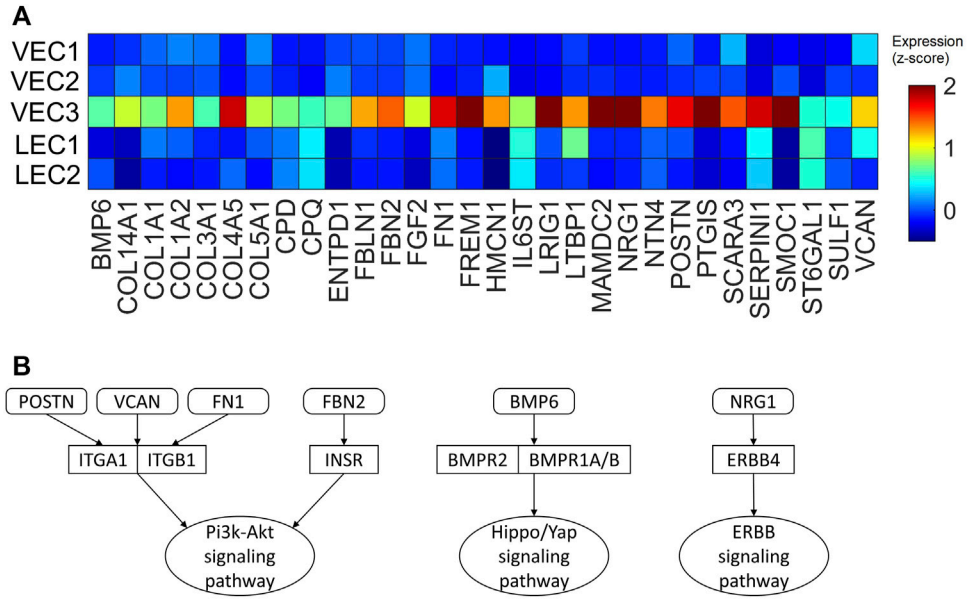

FIGURE 9
Upregulated genes encoding secretable proteins in cluster VEC3 interact with receptors of signaling pathways enriched in the regenerative hearts. **(A)** Heatmap of 30 genes encoding secretable proteins that exclusively upregulated (fold-change >2) in cluster VEC3; here, the expression is scaled by z-score and reflected in the heatmap color. **(B)** Protein-protein interactions, which were queried from BioGrid database, between the genes and their receptors of Pi3k-Akt, Hippo/YAP, and ERRB4 signaling pathways; round rectangle: genes; rectangle: signaling pathway receptors; oval: downstream signaling pathway.

Furthermore, NRG1 interacts with ERBB4, and Bone Morphogenetic Protein 6 [BMP6] interacts with receptors Bone Morphogenetic Protein Receptor Type 1A/B and Type 2 [BMPR1A/B, BMPR2] of the Hippo/Yap signaling pathway. Overall, these secret protein-receptor interactions suggested that VEC3 cluster may promote cardiomyocyte proliferation and overall regeneration.

3 Discussion

ECs comprise an exceptionally heterogeneous population of cells with unique features and functions that are specialized for each organ, for each vascular category (i.e., arteries, veins, capillaries, lymph vessels) within an organ, and for each segment within a vessel (Becker et al., 2023). The rate of EC turnover is believed to be low in most healthy organs, but the cells rapidly proliferate in response to injury (Potente et al., 2011). Thus, as we sought to characterize how different subpopulations of ECs participate in the angiogenic response to MI, we analyzed snRNAseq data from ECs that were collected during previous studies in our neonatal pig cardiac double-injury ($AR_{P1}MI_{P28}$) model via our cell-cycle–specific AI Autoencoder. Our analysis distributed the cells into five EC clusters, three containing VECs and two containing LECs.

Of the three VEC clusters, only one (VEC1) was enriched for cell-cycle activity, while another (VEC3) highly expressed genes involved in cell adhesion, in the regulation of intercellular junctions, in the EndMT, and in TGFβ/BMP signaling, which regulates the EndMT (Piera-Velazquez and Jimenez, 2019). Notably, angiogenesis is initiated by vessel sprouting (Sun et al., 2016), which begins with the loss of junctions between ECs and may be accompanied by onset of the EndMT in tip cells (Gerhardt et al., 2003); then, ECs located in the stalk of the sprout proliferate to lengthen and expand the endothelial tube (Marcelo et al., 2013). Thus, our observations suggest that VEC3 ECs may function as EC tip cells, while the VEC1 cluster could be composed primarily of stalk ECs. Furthermore, while ECs of the VEC2 cluster did not appear to be directly involved in angiogenesis, our trajectory analyses identified pathways linking VEC2 to both VEC1 and VEC3, which suggests that the VEC2 cluster contains a reservoir of ECs that can transform into tip (VEC3) or stalk (VEC1) ECs during angiogenesis. This observation is consistent with reports (Tian et al., 2015) that proliferating ECs are generated primarily from pre-existing ECs rather than another source, but we did not find a trajectory between VEC1 and VEC3, so the onset of EC cell-cycle activity does not appear to be driven by the EndMT. Notably, LEC1 ECs were enriched for many of the same mitosis/cytokinesis markers, gene ontology terms, and transcription factors that were upregulated in VEC1 ECs, which suggests that they also proliferate in response to MI and, consequently, may limit cardiac edema by increasing the uptake of interstitial fluid, but their precise role during recovery from myocardial injury has yet to be investigated.

The EndMT has been linked to increases in fibrosis (Fan et al., 2023), and recent studies in mice suggest that the acquisition of a mesenchymal-like phenotype in ECs after MI can lead to vascular abnormalities in newly formed vessels that block the efficient delivery of oxygen and other nutrients to the myocardium (Huang et al., 2022). These reports may appear to conflict with our observation that VEC3 ECs, which expressed elevated levels of EndMT genes, were the only EC subpopulation that was enriched in regenerating hearts. However, this discrepancy may be at least partially explained by

differences in the prevalence and/or persistence of the mesenchymal-like phenotype: whereas the VEC3 cluster never contained more than ~7.5% of ECs in nonfetal pig hearts and was expanded for just 1 week after MI induction in $AR_{P1}MI_{P28}$ pigs, the proportion of ECs that expressed mesenchymal genes in infarcted mouse hearts (Huang et al., 2022) increased from 1%–3% to 20%–70% during the first week after MI induction, and 5%–20% of them continued to express at least some mesenchymal genes for 3–8 weeks afterward. On the other hand, EC acquiring the EndMT markers may enhance their ability to proliferate, migrate, and dissociate (Huang et al., 2022). Our vessel density analysis showed that 2 days following MI_{P28} injury, the regenerative heart vessel density, where the VEC3 cluster strongly presented, quickly reached the CTL-P28 level; meanwhile, the non-regenerative heart, with a very small amount of VEC3, vessel density did not. VEC3 may promote cardiomyocyte proliferation and overall heart generation by secreting pro-proliferative proteins.

In conclusion, our analyses of cardiac snRNAseq data collected from fetal pigs and pigs that underwent AR_{P1}, MI_{P28}, both AR_{P1} and MI_{P28}, or neither experimental injury identified three clusters of VECs and two LEC clusters. Cells from just one of the VEC clusters (VEC1) appeared to proliferate in response to MI induction, and a second VEC cluster (VEC3) was enriched for the expression of genes that regulate intercellular junctions, participate in TGFβ/BMP signaling and promote the EndMT, while the remaining VEC cluster (VEC2) appeared to provide a reservoir of ECs that transformed into VEC1 or VEC3 ECs after MI. Notably, although the roles of TGFβ/BMP signaling and the EndMT have been well-studied in cardiac development, their involvement in cardiac regeneration is not well understood. Thus, more in-depth studies of the VEC3 cluster could identify new targets for improving the regeneration of infarcted hearts.

4 Methods

4.1 snRNAseq datasets

The pig snRNAseq dataset was obtained from the Gene Expression Omnibus database (accession number GSE185289). The complete dataset included 250,700 cells and was processed as described previously (Nakada et al., 2022; Nguyen et al., 2022; Nguyen et al., 2023b). The number of pig hearts for each group was summarized in Supplementary Table S3. The data were normalized with Seurat v.4 (Hao et al., 2021); then, expression data for 14,753 genes with at least 1,000 unique molecular identifiers were embedded into 10 dimensions with an Autoencoder. The results were visualized via Uniform Manifold Approximation (UMAP), and clustering was performed with the UMAP density-based clustering (dbscan) algorithm (McInnes et al., 2018; Meehan, 2021). Cells in clusters that specifically expressed the EC markers PECAM1 and KDR were considered ECs. A total of 29,826 ECs were identified.

4.2 Animal heart tissues

Frozen tissues, from which the snRNAseq datasets (Nakada et al., 2022; Nguyen et al., 2022; Nguyen et al., 2023b) were generated, were cut into 1 cm thick sections, embedded in optimal cutting temperature compound, and preserved in −80°C freezers. All experimental protocols were approved by The Institutional Animal Care and Use Committee (IACUC) of the University of Alabama, Birmingham, and performed in accordance with the National Institutes of Health Guide for the Care and Use of Laboratory Animals (NIH publication No 85-23).

4.3 Cell-cycle-specific analyses

4.3.1 Autoencoder and clustering

EC data was extracted from the full pig dataset, and then snRNAseq data for the 1,646 genes associated with the Gene Ontology term "cell cycle" (GO:0007049) (Gene Ontology Annotations, 2022) were reprocessed via AI Autoencoding and cluster analysis. This cell-cycle-specific Autoencoder was composed of three layers: an input layer of 1,646 nodes (i.e., the snRNA expression data for each of the 1,646 cell-cycle genes), a hidden (embedded) layer of 10 nodes, and an output layer of 1,646 nodes. The input layer was alternately embedded into the hidden layer and expanded to form the output layer, and the similarity of the input and output layers was optimized by minimizing the following equation:

$$E = \frac{1}{N}\sum_{i}^{N}\sum_{j}^{N}\left(x_i - y_j\right)^2 + 0.001\|W\|^2 + Q \quad (1)$$

where N represents the number of ECs, x_i represents the cell-cycle–specific gene expression for an EC from the input layer, y_j represents the cell-cycle–specific gene expression for an EC from the output layer, $||W||^2$ represents the regularization of autoencoder weights, and Q represents the sparsity parameters (trainAutoencoder, 2021). Visualization and clustering were performed with the UMAP toolkit (McInnes et al., 2018; Meehan, 2021), and clusters of proliferating ECs were defined by co-enrichment for the expression of five proliferation markers (AURKB, MKI67, INCENP, CDCNA8, and BIRC5). We also conducted independent analysis using the entire genome (Supplementary Note S1) and other clustering parameters (Supplementary Note S2) to confirmed that the cell-cycle-specific approach did not miss any specific EC subpopulations.

4.3.2 Trajectory analysis

Cell-cycle–specific trajectory and pseudotime analysis were performed by processing snRNAseq data for the 1,646 cell-cycle–specific genes with the Monocle (v.3) toolkit (Trapnell et al., 2014; Qiu et al., 2017), and pseudotime order was determined by the localization of Cyclin D1, AURKB, and MKI67 expression.

4.4 Identification of cluster-specific genes

Upregulated genes for each EC cluster were identified according to the following criteria: 1) a cluster p-value (Fisher's Exact test (Fisher, 1922)) of less than 10^{-6}, 2) expression by more than 25% of cells in the cluster, and 3) mean expression at least 2-fold greater than among ECs in other clusters. For transcription factors, which

are typically expressed in low abundance, criteria for upregulation were modified to 1) a cluster p-value of $<10^{-6}$, 2) expression by >10% of cluster cells, and 3) mean expression >2-fold greater than among cells in other clusters. The list of transcription factors was obtained from the Transcriptional Regulatory Relationships Unraveled by Sentence-based Text mining database (TRRUST) (Han et al., 2018) version 2, and the set of upregulated genes for each cluster was analyzed with the DAVID functional annotation tool (Huang da et al., 2009); only terms present in the Gene Ontology (Huntley et al., 2015) and KEGG (Kanehisa et al., 2017) categories were selected. To avoid false positives caused by multihypothesis testing, the selected results were required to have a Benjamini-adjusted (Li and Barber, 2019) $p < 0.05$.

4.5 Immunohistochemistry studies

The immunofluorescence analyses were conducted similar to our previous work in (Nakada et al., 2022). Briefly, samples were cut into transverse sections (thickness: 10 μm), embedded into slides, washed in PBS, and fixed in 4% paraformaldehyde for 20 min at room temperature. Then, the slides were permeabilized at 4°C, 0.1% triton-x for 10 min, and then blocked with Ultra-V block for 7 min. Samples were incubated with mouse anti- PECAM1 at 1:100 (MCA1738, BioRad, United States) or rabbit anti Ki67 (1: 100 dilution, ab15580, Abcam, United States), or rabbit antiPDGFRA (1:100 dilution, AF0241, Affinity, United States), or rabbit anti-PLVAP (1:100 dilution, AF0241, Affinity), in PBS containing 10% goat serum (10% PBS)for overnight at 4°C. On the next day, donkey anti-mouse IgG conjugated with FITC at 1: 200 dilution and donkey anti-rabbit IgG conjugated with Cy3 at 1; 200 dilution were added for 1 h at room temperature Then, samples were washed after 1:1000 DAPI solution was added for 1 min, mounted in vectorshieldand cover slide for imaging.

The slides were put into an Olympus IX83 microscope to capture images. The image frame size was 1360-width × 1024-height pixels. Exposure time for PECAM1 fluorescence (green) was initially set to 2.8 s, and could be case-by-case adjusted between 2.6 and 3.2 s. Exposure time for Ki67 and PLVAP fluorescence (red) was initially set to 1.2s, and could be adjusted between 0.9 and 1.4 s. Exposure time for PDGFRA fluorescence (red) was always set to 1.2s. DAPI (blue) exposure time was between 12 and 18 μs. Z-stack parameter was set to 0 for all images and channels. For each slide, ten image sets were captured; each image set include three channels: red, green, and blue; then, the three-channels were put together by Matlab to create a 'merge' RGB-color image.

Three-channel images (green: PECAM1; red: either Ki67, PDGFRA, or PLVAP; blue: DAPI) were processed using Matlab as in (Nguyen et al., 2022). Multi-thresholding segmentation method (Otsu, 1979) (Matlab multithresh function) was applied to extract image fluorescence regions. The vessel density was computed as the percentage of image area with green fluorescence. EC nuclei were recognized as the DAPI (blue) blocks overlapping with green regions; EC proliferating cells were recognized as the Ki67 red block overlapping with green regions; and EC proliferation marker was computed by the ratio between EC proliferating cells and EC DAPI. EC PDGFRA expression was assessed by the average red intensity overlapping with green fluorescence. For PLVAP + EC analysis, the PECAM1 and PLVAP fluorescence intensity was amplified by 2x before merging into one 3D image channel, PLVAP signal that were not overlapping with PECAM1 was removed for enhanced visualization (PLVAP/DAPI/PECAM1(e) images); then, the number of PLVAP + ECs was manually counted. Statistical comparison among the groups was completed using non-parametric Wilcoxon's Ranksum test. A p-value < 0.05 indicates statistical significance.

Data availability statement

The original contributions presented in the study are included in the article/Supplementary Material; the analytic program is provided at https://github.com/thamnguy/Cardiac-endothelial-cell; further inquiries can be directed to the corresponding author.

Ethics statement

The animal study was approved by the Institutional Animal Care and Use Committee (IACUC) of the University of Alabama, Birmingham, and performed in accordance with the National Institutes of Health Guide for the Care and Use of Laboratory Animals (NIH publication No. 85-23). The study was conducted in accordance with the local legislation and institutional requirements.

Author contributions

TN: Formal Analysis, Methodology, Investigation, Writing–original draft, XG: Investigation, Writing–review and editing, YW: Investigation, Writing–review and editing, LY: Methodology, Writing–review and editing, DG: Conceptualization, Writing–review and editing. JZ: Conceptualization, Funding acquisition, Supervision, Writing–review and editing.

Funding

The author(s) declare financial support was received for the research, authorship, and/or publication of this article. This work was supported by the following funding sources: NIH RO1s HL138990, HL114120, HL 131017, HL149137, UO1 HL134764, and P01 HL160476.

Conflict of interest

The authors declare that the research was conducted in the absence of any commercial or financial relationships that could be construed as a potential conflict of interest.

The reviewer AQ declared a past co-authorship with the author JZ to the handling editor.

The author(s) declared that they were an editorial board member of Frontiers, at the time of submission. This had no impact on the peer review process and the final decision.

Publisher's note

Supplementary material

The Supplementary Material for this article can be found online at: https://www.frontiersin.org/articles/10.3389/fbioe.2023.1257669/full#supplementary-material

SUPPLEMENTARY TABLE S1
Summary of upregulated genes, pathways, and biological processes in VEC1. **(A)** Gene expression is summarized as the proportion of VEC1 ECs that express the gene, the fold-change in gene expression relative to expression in non-VEC1 ECs, and the *p*-value (Fisher's Exact test). **(B)** Expression of genes in **(A)** was processed with the DAVID toolkit (https://david.ncifcrf.gov/) to identify pathways and biological processes that were enriched in VEC1; the enrichment *p*-value was corrected to control for false-discoveries.

SUPPLEMENTAL TABLE S2
Summary of upregulated genes, pathways, and biological processes in VEC3. **(A)** Gene expression is summarized as the proportion of VEC3 ECs that express the gene, the fold-change in gene expression relative to expression in non-VEC3 ECs, and the *p*-value (Fisher's Exact test). **(B)** Expression of genes in **(A)** was processed with the DAVID toolkit (https://david.ncifcrf.gov/) to identify pathways and biological processes that were enriched in VEC3; the enrichment *p*-value was corrected to control for false-discoveries.

SUPPLEMENTAL TABLE S3
Sample size *n* (number of pig hearts) per each sample group in our study. The first column indicates the animal group (injury & timepoints), including n. The second column indicates the heart identification. The third and fourth columns indicate whether the heart underwent apical resection on P1 and/or myocardial infarction on P28. The last column indicates the age (day) when the heart tissues were harvested.

References

Banerji, S., Ni, J., Wang, S. X., Clasper, S., Su, J., Tammi, R., et al. (1999). LYVE-1, a new homologue of the CD44 glycoprotein, is a lymph-specific receptor for hyaluronan. *J. Cell. Biol.* 144, 789–801. doi:10.1083/jcb.144.4.789

Bass-Zubek, A. E., Hobbs, R. P., Amargo, E. V., Garcia, N. J., Hsieh, S. N., Chen, X., et al. (2008). Plakophilin 2: a critical scaffold for PKC alpha that regulates intercellular junction assembly. *J. Cell. Biol.* 181, 605–613. doi:10.1083/jcb.200712133

Becker, L. M., Chen, S. H., Rodor, J., de Rooij, L., Baker, A. H., and Carmeliet, P. (2023). Deciphering endothelial heterogeneity in health and disease at single-cell resolution: progress and perspectives. *Cardiovasc Res.* 119, 6–27. doi:10.1093/cvr/cvac018

Bersell, K., Arab, S., Haring, B., and Kuhn, B. (2009). Neuregulin1/ErbB4 signaling induces cardiomyocyte proliferation and repair of heart injury. *Cell.* 138, 257–270. doi:10.1016/j.cell.2009.04.060

Bloomekatz, J., Singh, R., Prall, O. W., Dunn, A. C., Vaughan, M., Loo, C. S., et al. (2017). Platelet-derived growth factor (PDGF) signaling directs cardiomyocyte movement toward the midline during heart tube assembly. *Elife* 6, e21172. doi:10.7554/elife.21172

Chakraborty, S., Sengupta, A., and Yutzey, K. E. (2013). Tbx20 promotes cardiomyocyte proliferation and persistence of fetal characteristics in adult mouse hearts. *J. Mol. Cell. Cardiol.* 62, 203–213. doi:10.1016/j.yjmcc.2013.05.018

Chakraborty, S., and Yutzey, K. E. (2012). Tbx20 regulation of cardiac cell proliferation and lineage specialization during embryonic and fetal development *in vivo*. *Dev. Biol.* 363, 234–246. doi:10.1016/j.ydbio.2011.12.034

Chen, Q., Yu, W. Y., Zhang, H. H., Zhang, S. Z., Fang, J., Wu, F., et al. (2020). PBX3 promotes tumor growth and angiogenesis via activation of at1r/VEGFR2 pathway in papillary thyroid carcinoma. *Biomed. Res. Int.* 2020, 1–10. doi:10.1155/2020/8954513

Chiong, M., Wang, Z. V., Pedrozo, Z., Cao, D. J., Troncoso, R., Ibacache, M., et al. (2011). Cardiomyocyte death: mechanisms and translational implications. *Cell. Death Dis.* 2, e244. doi:10.1038/cddis.2011.130

Denzer, L., Muranyi, W., Schroten, H., and Schwerk, C. (2023). The role of PLVAP in endothelial cells. *Cell. Tissue Res.* 392, 393–412. doi:10.1007/s00441-023-03741-1

Diebold, L. P., Gil, H. J., Gao, P., Martinez, C. A., Weinberg, S. E., and Chandel, N. S. (2019). Mitochondrial complex III is necessary for endothelial cell proliferation during angiogenesis. *Nat. Metab.* 1, 158–171. doi:10.1038/s42255-018-0011-x

Fan, M., Yang, K., Wang, X., Chen, L., Gill, P. S., Ha, T., et al. (2023). Lactate promotes endothelial-to-mesenchymal transition via Snail1 lactylation after myocardial infarction. *Sci. Adv.* 9, eadc9465. doi:10.1126/sciadv.adc9465

Feng, J., Li, Y., Li, Y., Yin, Q., Li, H., Li, J., et al. (2023). Versican promotes cardiomyocyte proliferation and cardiac repair. *Circulation*. doi:10.1161/circulationaha.123.066298

Fina, L., Molgaard, H. V., Robertson, D., Bradley, N. J., Monaghan, P., Delia, D., et al. (1990). Expression of the CD34 gene in vascular endothelial cells. *Blood* 75, 2417–2426. doi:10.1182/blood.v75.12.2417.bloodjournal75122417

Fisher, R. A. (1922). On the interpretation of χ 2 from contingency tables, and the calculation of P. *J. R. Stat. Soc.* 85, 87–94. doi:10.2307/2340521

Gemberling, M., Karra, R., Dickson, A. L., and Poss, K. D. (2015). Nrg1 is an injury-induced cardiomyocyte mitogen for the endogenous heart regeneration program in zebrafish. *Elife* 4, e05871. doi:10.7554/elife.05871

Gene Ontology Annotations (2022). *Cell cycle*. China: Mouse Genome Informatics.

Gene Ontology Annotations (2023a). BMP signaling pathway. *Mouse Genome Inf.*

Gene Ontology Annotations (2023b). *DNA repair, mouse genome informatics.*

Gene Ontology Annotations (2023c). Mitotic chromosome condensation. *Mouse Genome Inf.*

Gerhardt, H., Golding, M., Fruttiger, M., Ruhrberg, C., Lundkvist, A., Abramsson, A., et al. (2003). VEGF guides angiogenic sprouting utilizing endothelial tip cell filopodia. *J. Cell. Biol.* 161, 1163–1177. doi:10.1083/jcb.200302047

Giannotta, M., Trani, M., and Dejana, E. (2013). VE-cadherin and endothelial adherens junctions: active guardians of vascular integrity. *Dev. Cell.* 26, 441–454. doi:10.1016/j.devcel.2013.08.020

Gordon, K. J., and Blobe, G. C. (2008). Role of transforming growth factor-beta superfamily signaling pathways in human disease. *Biochim. Biophys. Acta* 1782, 197–228. doi:10.1016/j.bbadis.2008.01.006

Han, H., Cho, J. W., Lee, S., Yun, A., Kim, H., Bae, D., et al. (2018). TRRUST v2: an expanded reference database of human and mouse transcriptional regulatory interactions. *Nucleic Acids Res.* 46, D380–D386. doi:10.1093/nar/gkx1013

Hao, Y., Hao, S., Andersen-Nissen, E., Mauck, W. M., 3rd, Zheng, S., Butler, A., et al. (2021). Integrated analysis of multimodal single-cell data. *Cell.* 184, 3573–3587 e29. doi:10.1016/j.cell.2021.04.048

Harel, S., Sanchez, V., Moamer, A., Sanchez-Galan, J. E., Abid Hussein, M. N., Mayaki, D., et al. (2021). ETS1, ELK1, and ETV4 transcription factors regulate angiopoietin-1 signaling and the angiogenic response in endothelial cells. *Front. Physiol.* 12, 683651. doi:10.3389/fphys.2021.683651

Huang, M., Yang, F., Zhang, D., Lin, M., Duan, H., El-Mayta, R., et al. (2022). Endothelial plasticity drives aberrant vascularization and impedes cardiac repair after myocardial infarction. *Nat. Cardiovasc Res.* 1, 372–388. doi:10.1038/s44161-022-00047-3

Huang da, W., Sherman, B. T., and Lempicki, R. A. (2009). Systematic and integrative analysis of large gene lists using DAVID bioinformatics resources. *Nat. Protoc.* 4, 44–57. doi:10.1038/nprot.2008.211

Huntley, R. P., Sawford, T., Mutowo-Meullenet, P., Shypitsyna, A., Bonilla, C., Martin, M. J., et al. (2015). The Goa database: gene Ontology annotation updates for 2015. *Nucleic Acids Res.* 43, D1057–D1063. doi:10.1093/nar/gku1113

Ingason, A. B., Goldstone, A. B., Paulsen, M. J., Thakore, A. D., Truong, V. N., Edwards, B. B., et al. (2018). Angiogenesis precedes cardiomyocyte migration in regenerating mammalian hearts. *J. Thorac. Cardiovasc Surg.* 155, 1118–1127 e1. doi:10.1016/j.jtcvs.2017.08.127

Johnson, K. E., and Wilgus, T. A. (2014). Vascular endothelial growth factor and angiogenesis in the regulation of cutaneous wound repair. *Adv. Wound Care (New Rochelle)* 3, 647–661. doi:10.1089/wound.2013.0517

Johnson, L. A., and Jackson, D. G. (2010). Inflammation-induced secretion of CCL21 in lymphatic endothelium is a key regulator of integrin-mediated dendritic cell transmigration. *Int. Immunol.* 22, 839–849. doi:10.1093/intimm/dxq435

Kanehisa, M., Furumichi, M., Tanabe, M., Sato, Y., and Morishima, K. (2017). KEGG: new perspectives on genomes, pathways, diseases and drugs. *Nucleic Acids Res.* 45, D353–D361. doi:10.1093/nar/gkw1092

KEGG (2023). *TGF-beta signaling pathway* - Sus scrofa *(pig)*. Kyoto University.

Khurana, R., Simons, M., Martin, J. F., and Zachary, I. C. (2005). Role of angiogenesis in cardiovascular disease: a critical appraisal. *Circulation* 112, 1813–1824. doi:10.1161/circulationaha.105.535294

Kovacic, J. C., Dimmeler, S., Harvey, R. P., Finkel, T., Aikawa, E., Krenning, G., et al. (2019). Endothelial to mesenchymal transition in cardiovascular disease: JACC state-of-the-art review. *J. Am. Coll. Cardiol.* 73, 190–209. doi:10.1016/j.jacc.2018.09.089

Kuhn, B., del Monte, F., Hajjar, R. J., Chang, Y. S., Lebeche, D., Arab, S., et al. (2007). Periostin induces proliferation of differentiated cardiomyocytes and promotes cardiac repair. *Nat. Med.* 13, 962–969. doi:10.1038/nm1619

Laflamme, M. A., and Murry, C. E. (2011). Heart regeneration. *Nature* 473, 326–335. doi:10.1038/nature10147

Li, A., and Barber, R. F. (2019). Multiple testing with the structure-adaptive Benjamini–Hochberg algorithm. *J. R. Stat. Soc. Ser. B Stat. Methodol.* 81, 45–74. doi:10.1111/rssb.12298

Li, F., Ambrosini, G., Chu, E. Y., Plescia, J., Tognin, S., Marchisio, P. C., et al. (1998). Control of apoptosis and mitotic spindle checkpoint by survivin. *Nature* 396, 580–584. doi:10.1038/25141

Lu, L., Liu, M., Sun, R., Zheng, Y., and Zhang, P. (2015). Myocardial infarction: symptoms and treatments. *Cell. Biochem. Biophys.* 72, 865–867. doi:10.1007/s12013-015-0553-4

Maitra, M., Schluterman, M. K., Nichols, H. A., Richardson, J. A., Lo, C. W., Srivastava, D., et al. (2009). Interaction of Gata4 and Gata6 with Tbx5 is critical for normal cardiac development. *Dev. Biol.* 326, 368–377. doi:10.1016/j.ydbio.2008.11.004

Marcelo, K. L., Goldie, L. C., and Hirschi, K. K. (2013). Regulation of endothelial cell differentiation and specification. *Circ. Res.* 112, 1272–1287. doi:10.1161/circresaha.113.300506

Martinou, E. G., Moller-Levet, C. S., and Angelidi, A. M. (2022). PBX4 functions as a potential novel oncopromoter in colorectal cancer: a comprehensive analysis of the PBX gene family. *Am. J. Cancer Res.* 12, 585–600.

McInnes, L., Healy, J., and Melville, J., UMAP: Uniform manifold approximation and projection for dimension reduction. arXiv preprint arXiv:1802.03426 (2018).

McMullen, J. R., and Jennings, G. L. (2007). Differences between pathological and physiological cardiac hypertrophy: novel therapeutic strategies to treat heart failure. *Clin. Exp. Pharmacol. Physiol.* 34, 255–262. doi:10.1111/j.1440-1681.2007.04585.x

Meehan, S. (2021). *Uniform Manifold approximation and projection*. USA: UMAP.

Misra, C., Chang, S. W., Basu, M., Huang, N., and Garg, V. (2014). Disruption of myocardial Gata4 and Tbx5 results in defects in cardiomyocyte proliferation and atrioventricular septation. *Hum. Mol. Genet.* 23, 5025–5035. doi:10.1093/hmg/ddu215

Morrell, N. W., Bloch, D. B., ten Dijke, P., Goumans, M. J., Hata, A., Smith, J., et al. (2016). Targeting BMP signalling in cardiovascular disease and anaemia. *Nat. Rev. Cardiol.* 13, 106–120. doi:10.1038/nrcardio.2015.156

Nakada, Y., Zhou, Y., Gong, W., Zhang, E. Y., Skie, E., Nguyen, T., et al. (2022). Single nucleus transcriptomics: apical resection in newborn pigs extends the time window of cardiomyocyte proliferation and myocardial regeneration. *Circulation* 145, 1744–1747. doi:10.1161/circulationaha.121.056995

Newman, P. J. (1994). The role of PECAM-1 in vascular cell biology[a]. *Ann. N. Y. Acad. Sci.* 714, 165–174. doi:10.1111/j.1749-6632.1994.tb12041.x

Nguyen, T., Wei, Y., Nakada, Y., Chen, J. Y., Zhou, Y., Walcott, G., et al. (2023a). Analysis of cardiac single-cell RNA-sequencing data can be improved by the use of artificial-intelligence-based tools. *Sci. Rep.* 13, 6821. doi:10.1038/s41598-023-32293-1

Nguyen, T., Wei, Y., Nakada, Y., Chen, J. Y., Zhou, Y., Walcott, G., et al. (2023b). Analysis of cardiac single-cell RNA-sequencing data can be improved by the use of artificial-intelligence-based tools. *Sci. Rep.* 13, 6821. doi:10.1038/s41598-023-32293-1

Nguyen, T., Wei, Y., Nakada, Y., Zhou, Y., and Zhang, J. (2022). Cardiomyocyte cell-cycle regulation in neonatal large mammals: single nucleus RNA-sequencing data analysis via an artificial-intelligence-based pipeline. *Front. Bioeng. Biotechnol.* 10, 914450. doi:10.3389/fbioe.2022.914450

Otsu, N. (1979). A threshold selection method from gray-level histograms. *IEEE Trans. Syst. Man, Cybern.* 9, 62–66. doi:10.1109/tsmc.1979.4310076

Oughtred, R., Rust, J., Chang, C., Breitkreutz, B. J., Stark, C., Willems, A., et al. (2021). The BioGRID database: a comprehensive biomedical resource of curated protein, genetic, and chemical interactions. *Protein Sci.* 30, 187–200. doi:10.1002/pro.3978

Piera-Velazquez, S., and Jimenez, S. A. (2019). Endothelial to mesenchymal transition: role in physiology and in the pathogenesis of human diseases. *Physiol. Rev.* 99, 1281–1324. doi:10.1152/physrev.00021.2018

Planutiene, M., Planutis, K., and Holcombe, R. F. (2011). Lymphoid enhancer-binding factor 1, a representative of vertebrate-specific Lef1/Tcf1 sub-family, is a Wnt-beta-catenin pathway target gene in human endothelial cells which regulates matrix metalloproteinase-2 expression and promotes endothelial cell invasion. *Vasc. Cell.* 3, 28. doi:10.1186/2045-824x-3-28

Porrello, E. R., Mahmoud, A. I., Simpson, E., Hill, J. A., Richardson, J. A., Olson, E. N., et al. (2011). Transient regenerative potential of the neonatal mouse heart. *Science* 331, 1078–1080. doi:10.1126/science.1200708

Potente, M., Gerhardt, H., and Carmeliet, P. (2011). Basic and therapeutic aspects of angiogenesis. *Cell.* 146, 873–887. doi:10.1016/j.cell.2011.08.039

Prabhu, S. D., and Frangogiannis, N. G. (2016). The biological basis for cardiac repair after myocardial infarction: from inflammation to fibrosis. *Circ. Res.* 119, 91–112. doi:10.1161/circresaha.116.303577

Qin, G., Kishore, R., Dolan, C. M., Silver, M., Wecker, A., Luedemann, C. N., et al. (2006). Cell cycle regulator E2F1 modulates angiogenesis via p53-dependent transcriptional control of VEGF. *Proc. Natl. Acad. Sci. U. S. A.* 103, 11015–11020. doi:10.1073/pnas.0509533103

Qiu, X., Mao, Q., Tang, Y., Wang, L., Chawla, R., Pliner, H. A., et al. (2017). Reversed graph embedding resolves complex single-cell trajectories. *Nat. Methods* 14, 979–982. doi:10.1038/nmeth.4402

Singh, S., Prakash, S., and Gupta, S. K. (2022). Angiogenesis: a critical determinant for cardiac regeneration. *Mol. Ther. Nucleic Acids* 29, 88–89. doi:10.1016/j.omtn.2022.06.007

Smits, M., Wurdinger, T., van het Hof, B., Drexhage, J. A., Geerts, D., Wesseling, P., et al. (2012). Myc-associated zinc finger protein (MAZ) is regulated by miR-125b and mediates VEGF-induced angiogenesis in glioblastoma. *FASEB J.* 26, 2639–2647. doi:10.1096/fj.11-202820

Steinhauser, M. L., and Lee, R. T. (2011). Regeneration of the heart. *EMBO Mol. Med.* 3, 701–712. doi:10.1002/emmm.201100175

Sun, X., Altalhi, W., and Nunes, S. S. (2016). Vascularization strategies of engineered tissues and their application in cardiac regeneration. *Adv. Drug Deliv. Rev.* 96, 183–194. doi:10.1016/j.addr.2015.06.001

Sutton, M. G., and Sharpe, N. (2000). Left ventricular remodeling after myocardial infarction: pathophysiology and therapy. *Circulation* 101, 2981–2988. doi:10.1161/01.cir.101.25.2981

Tan, C. M. J., and Lewandowski, A. J. (2020). The transitional heart: from early embryonic and fetal development to neonatal life. *Fetal Diagn Ther.* 47, 373–386. doi:10.1159/000501906

Terman, B. I., Dougher-Vermazen, M., Carrion, M. E., Dimitrov, D., Armellino, D. C., Gospodarowicz, D., et al. (1992). Identification of the KDR tyrosine kinase as a receptor for vascular endothelial cell growth factor. *Biochem. Biophys. Res. Commun.* 187, 1579–1586. doi:10.1016/0006-291x(92)90483-2

Tian, X., Hu, T., Zhang, H., He, L., Huang, X., Liu, Q., et al. (2014). *De novo* formation of a distinct coronary vascular population in neonatal heart. *Science* 345, 90–94. doi:10.1126/science.1251487

Tian, X., Pu, W. T., and Zhou, B. (2015). Cellular origin and developmental program of coronary angiogenesis. *Circ. Res.* 116, 515–530. doi:10.1161/circresaha.116.305097

trainAutoencoder (2021). *trainAutoencoder, Mathworks*. USA: Inc.

Trapnell, C., Cacchiarelli, D., Grimsby, J., Pokharel, P., Li, S., Morse, M., et al. (2014). The dynamics and regulators of cell fate decisions are revealed by pseudotemporal ordering of single cells. *Nat. Biotechnol.* 32, 381–386. doi:10.1038/nbt.2859

Vader, G., Medema, R. H., and Lens, S. M. (2006). The chromosomal passenger complex: guiding Aurora-B through mitosis. *J. Cell. Biol.* 173, 833–837. doi:10.1083/jcb.200604032

Wang, J., Karra, R., Dickson, A. L., and Poss, K. D. (2013). Fibronectin is deposited by injury-activated epicardial cells and is necessary for zebrafish heart regeneration. *Dev. Biol.* 382, 427–435. doi:10.1016/j.ydbio.2013.08.012

Weijts, B. G., Bakker, W. J., Cornelissen, P. W., Liang, K. H., Schaftenaar, F. H., Westendorp, B., et al. (2012). E2F7 and E2F8 promote angiogenesis through transcriptional activation of VEGFA in cooperation with HIF1. *EMBO J.* 31, 3871–3884. doi:10.1038/emboj.2012.231

Wigle, J. T., Harvey, N., Detmar, M., Lagutina, I., Grosveld, G., Gunn, M. D., et al. (2002). An essential role for Prox1 in the induction of the lymphatic endothelial cell phenotype. *EMBO J.* 21, 1505–1513. doi:10.1093/emboj/21.7.1505

Wu, J., Meng, X., Jia, Y., Chai, J., Wang, J., Xue, X., et al. (2020). Long non-coding RNA HNF1A-AS1 upregulates OTX1 to enhance angiogenesis in colon cancer via the binding of transcription factor PBX3. *Exp. Cell. Res.* 393, 112025. doi:10.1016/j.yexcr.2020.112025

Wu, X., Reboll, M. R., Korf-Klingebiel, M., and Wollert, K. C. (2021). Angiogenesis after acute myocardial infarction. *Cardiovasc Res.* 117, 1257–1273. doi:10.1093/cvr/cvaa287

Xiang, F. L., Guo, M., and Yutzey, K. E. (2016). Overexpression of Tbx20 in adult cardiomyocytes promotes proliferation and improves cardiac function after myocardial infarction. *Circulation* 133, 1081–1092. doi:10.1161/circulationaha.115.019357

Yan, W., Han, Q., Gong, L., Zhan, X., Li, W., Guo, Z., et al. (2022). MBD3 promotes hepatocellular carcinoma progression and metastasis through negative regulation of tumour suppressor TFPI2. *Br. J. Cancer* 127, 612–623. doi:10.1038/s41416-022-01831-5

Yao, L., Rathnakar, B. H., Kwon, H. R., Sakashita, H., Kim, J. H., Rackley, A., et al. (2022). Temporal control of PDGFRα regulates the fibroblast-to-myofibroblast transition in wound healing. *Cell. Rep.* 40, 111192. doi:10.1016/j.celrep.2022.111192

Ye, L., D'Agostino, G., Loo, S. J., Wang, C. X., Su, L. P., Tan, S. H., et al. (2018). Early regenerative capacity in the porcine heart. *Circulation* 138, 2798–2808. doi:10.1161/circulationaha.117.031542

Zhang, E., Nguyen, T., Zhao, M., Dang, S. D. H., Chen, J. Y., Bian, W., et al. (2020). Identifying the key regulators that promote cell-cycle activity in the hearts of early neonatal pigs after myocardial injury. *PLoS One* 15, e0232963. doi:10.1371/journal.pone.0232963

Zhang, R., Wang, N., Zhang, L. N., Huang, N., Song, T. F., Li, Z. Z., et al. (2016). Knockdown of DNMT1 and DNMT3a promotes the angiogenesis of human mesenchymal stem cells leading to arterial specific differentiation. *Stem Cells* 34, 1273–1283. doi:10.1002/stem.2288

Zhao, M., Zhang, E., Wei, Y., Zhou, Y., Walcott, G. P., and Zhang, J. (2020). Apical resection prolongs the cell cycle activity and promotes myocardial regeneration after left ventricular injury in neonatal pig. *Circulation* 142, 913–916. doi:10.1161/circulationaha.119.044619

Zhao, Y. Y., Gao, X. P., Zhao, Y. D., Mirza, M. K., Frey, R. S., Kalinichenko, V. V., et al. (2006). Endothelial cell-restricted disruption of FoxM1 impairs endothelial repair following LPS-induced vascular injury. *J. Clin. Investig.* 116, 2333–2343. doi:10.1172/jci27154

Zhou, J., Cheng, M., Wu, M., Boriboun, C., Jujo, K., Xu, S., et al. (2013). Contrasting roles of E2F2 and E2F3 in endothelial cell growth and ischemic angiogenesis. *J. Mol. Cell. Cardiol.* 60, 68–71. doi:10.1016/j.yjmcc.2013.04.009

Zhu, J., Wu, Y., Yu, Y., Li, Y., Shen, J., and Zhang, R. (2022). MYBL1 induces transcriptional activation of ANGPT2 to promote tumor angiogenesis and confer sorafenib resistance in human hepatocellular carcinoma. *Cell. Death Dis.* 13, 727. doi:10.1038/s41419-022-05180-2

Zhu, W., Zhang, E., Zhao, M., Chong, Z., Fan, C., Tang, Y., et al. (2018). Regenerative potential of neonatal porcine hearts. *Circulation* 138, 2809–2816. doi:10.1161/circulationaha.118.034886